Urban Climate 19 (2017) 1–27

Contents lists available at ScienceDirect

Urban Climate

journal homepage: http://www.elsevier.com/locate/uclim

Urban resilience to future urban heat waves under a climate change scenario: A case study for Porto urban area (Portugal)

D. Carvalho [a,*,1], H. Martins [a], M. Marta-Almeida [b], A. Rocha [b], C. Borrego [a]

[a] CESAM - Department of Environment and Planning, University of Aveiro, Campus Universitário de Santiago, 3810-193 Aveiro, Portugal
[b] CESAM - Department of Physics, University of Aveiro, Campus Universitário de Santiago, 3810-193 Aveiro, Portugal

ARTICLE INFO

Article history:
Received 3 February 2016
Received in revised form 21 September 2016
Accepted 21 November 2016

Keywords:
Heat resilience
Green roofs
White roofs
Urban parks
Urban atlas
CORINE land cover

ABSTRACT

This work aimed to assess the effectiveness of several resilience strategies to mitigate extreme urban heat episodes in Porto (Portugal). Different resilience scenarios were studied with the WRF urban modelling system, using as case-study a future heat wave occurring in Porto urban area. The resilience factors considered were the increase of urban green areas and the application of cool (green and white) roofs. The results showed that the most effective resilience strategies to mitigate high urban temperatures are the application of cool roofs. These resilience strategies produced the strongest reduction in the average and maximum surface temperatures over Porto urban area under a future heat wave. Considering that white roofs are considerably easier and cheaper to apply in urban areas than green roofs, this resilience strategy can be seen as the most viable, cost-effective and economically attractive approach for mitigating extreme urban temperatures.
This study proposed several different urban resilience strategies to extreme temperature episodes for the first time for Porto urban area, proved their effectiveness and compared their ability to reduce urban heat. Such findings can be of great importance for Porto urban planning stakeholders given the expected increase in the heat waves frequency and intensity in future climate.

* Corresponding author.
E-mail addresses: david.carvalho@ua.pt, david.carvalho@nasa.gov (D. Carvalho), hmartins@ua.pt (H. Martins), mma@ua.pt (M. Marta-Almeida), alfredo.rocha@ua.pt (A. Rocha), c.borrego@ua.pt (C. Borrego).
[1] Global Modeling and Assimilation Office (GMAO), NASA Goddard Space Flight Center, Greenbelt, MD, USA, Goddard Earth Sciences Technology and Research (GESTAR), Universities Space Research Association (USRA), Columbia, MD, USA.

http://dx.doi.org/10.1016/j.uclim.2016.11.005
2212-0955

1. Introduction

Currently over 70% of the European population live in cities, and this figure is expected to rise to more than 80% in the upcoming decades. By 2050, this means over 36 million new urban citizens. In Portugal, the current urban population is 61% (6 million) of the total population and is expected to grow to 75% by 2050, representing 1.4 million new inhabitants in Portuguese cities, mainly within Lisbon and Porto urban areas. Porto urban area, one of the largest and most densely populated urban areas in Portugal, represents almost 25% of Portugal in terms of its area and contains near 3.7 million inhabitants. It was identified as one of the European cities where the urban fringe has grown faster (EEA, 2011), resulting in a depletion of agricultural land and forests. At the same time, the latest Intergovernmental Panel on Climate Change (IPCC) Assessment Report (IPCC AR5, 2013) confirms the negative role of anthropogenic emissions on climate change, consequential to the daily life of citizens. Despite the global efforts to mitigate climate change, its negative effects are already underway and the future scenario is grim. Several authors refer changes in the regime of extreme weather events (including heavy rain, storms, tropical cyclones, drought, floods and heat waves), which will become more frequent and severe (Kharin and Zwiers, 2000; Santos and Corte-Real, 2006). One of the most worrisome is the occurrence of heat waves, due to their negative impacts on public health in urban areas (Monteiro et al., 2012). Specifically for Porto, Monteiro et al. (2013) related excess mortality and morbidity with the occurrence of a heat wave in July 2006. Watkiss et al. (2009) reported that the death rate related to extreme heat episodes in Europe could double by 2040 and even increase up to ten times by the end of the current century, with southern Europe experiencing the highest increases in the summer. More recently, Lau et al. (2015) reported that anthropogenic climate changes would likely increase the frequency, duration and magnitude of severe heat stress events mainly in highly populated urban areas, being Porto one of the cities that can expect the exacerbation of future heat waves.

Besides these meteorological extreme events, urban environments are usually exposed to higher ambient and surface temperatures when compared to their rural, or less urbanized, surroundings. Urban built surfaces, mainly composed of materials with low solar radiation reflectance and high heat storage capacities such as concrete and asphalt, build up significant amounts of sensible heat during the day that is released during the night to their surroundings. This originates a strong thermal gradient between the urban area (warmer) and its surroundings (cooler), an effect known as urban heat island (UHI). Although heat waves and UHI are two distinct meteorological phenomena, given that a heat wave typically results from large-scale, stagnant, high pressure systems that produce a temporal temperature anomaly for an entire region (urban and/or rural), while an UHI is a local process that occurs due to the different characteristics between urban and rural terrain (albedo, heat capacity and fluxes, land use), several studies showed that heat waves and UHI episodes are strongly connected and that, not only heat waves increase the ambient temperatures, but they also intensify UHI effects (Basara et al., 2010; Cheval et al., 2009; Founda et al., 2015). Li and Bou-Zeid (2013) showed that heat waves are expected to become more frequent, intense and long-lasting under a warming climate, and their non-linear interaction with UHI will originate extreme heat stress events in urban environments. Furthermore, other urban issues such as air pollution and anthropogenic heat sources (traffic, industry, etc.) significantly increase the thermal load inside the urban canopy layer (Papangelis et al., 2012). This additional thermal stress will induce, in a snowball effect, higher energy consumption to cool the building's interior that will further release additional heat and air pollutants into the urban canopy layer (hot air exhaustion from air conditioning devices, higher greenhouse gases emissions due to higher energy consumptions, etc.).

Thus, the combination of rapid urban growth, urban characteristics that favour thermal stress and climate change poses critical challenges to urban environments, and highlights the need for investigating resilience measures to mitigate high urban temperatures (Borrego et al., 2015). The inclusion of urban green areas (such as city parks) and the application of cool (green and/or white) roofs in built-up surfaces are efficient strategies to lower urban temperatures (Susca, 2012). These types of resilience measures mainly rely on the reduction of sensible heat fluxes between the lower atmosphere and the urban artificial surfaces (walls and roofs of buildings, roads and sidewalks surfaces, etc.). The ability of urban green areas and green roofs to reduce urban temperatures is mainly related to two properties of trees and vegetation: evapotranspiration and shading. While the first one cools the air by using heat from the air to evaporate the water (redirecting the energy to the form of latent heat, rather than sensible heat), the second allows the reduction of the solar radiation that reaches the area below the tree canopy. This cooler surface, in turn, reduces the heat transmitted into the surrounding buildings and atmosphere. The application of surfaces with high levels of solar reflectance, such as white roofs, increases the solar radiation reflection due to their higher albedo (Li et al.,

2014). Synnefa et al. (2008) reported that, for peak solar and low wind conditions, the temperature of a surface with an albedo of 0.05 is about 50 °C higher than the ambient air temperature. For a surface with an albedo of 0.8, the temperature difference drops down to about 10 °C. Besides improving the urban population thermal comfort, lowering urban temperatures means reducing energy consumption used for cooling. Moreover, vegetated areas bring many advantages to urban areas, such as air quality improvement and air pollution mitigation (CO_2 capture and O_2 production), reduction of the risk of urban floods through increased soil infiltration capacity (EEA, 2011), reduction of noise levels, biodiversity increase, and fostering the improvement of cultural, social and aesthetic issues by providing leisure, socialization and life quality in cities (EC, 2015). Furthermore, such measures can increase the number of attractive spaces in urban areas and act as a revitalizing factor for economically depressed areas (increase in tourism and commerce, for example).

Albeit the study of the application and effectiveness of such types of resilience measures to mitigate high urban temperatures is not novel in the published research, such study was never performed for Porto urban area, one of the urban areas most exposed to heat waves exacerbation due to climate changes (Lau et al., 2015), nor to any Portuguese city or urban environment. Studies such as Yang et al. (2015), Synnefa et al. (2008), Papangelis et al. (2012), Li et al. (2014) consistently reported the effectiveness and benefits of the application of resilience measures in urban heat mitigation in varied areas such as Beijing, Montréal, Phoenix, Vancouver, Athens, Baltimore-Washington metropolitan area, etc. Furthermore, the published research focuses on past-present extreme temperature episodes, and no study was found that addresses this issue under the light of the most recent IPCC CMIP5 future climate projections. Although Porto climate is relatively mild (in Summer temperatures rarely drift from the 15–25 °C range, while in Winter this range is of about 5–15 °C), it shows a high temperature and precipitation seasonality and inter-annual variability. This variability is aggravated by the poor building insulation and climatic suitability, leading to increased probability of severe human health consequences when extreme events such as heat waves occur (Monteiro and Velho, 2014). In addition, extreme meteorological events such as heat waves are rare and its population and urban fabric are not prepared or adapted to deal with such events, making their occurrence a serious and stressful problem. Furthermore, the projected future climate trends for this area are not encouraging: the studies of Borrego et al. (2015) and Marta-Almeida et al. (2016) showed that Porto urban area can expect an average increase of almost 2 °C in the medium-term future (2046–2065), which can almost double by the end of the current century (3.7 °C). These studies also show that in Porto urban area the heat waves frequency, duration and intensity are expected to substantially increase in the future, particularly for Summer periods. Although presently somewhat rare in terms of frequency and mild in terms of intensity and duration, it is expected that the occurrence of heat waves in Porto urban area can more than double by the medium-term future and increase by a factor of 3.6 in the long term future.

Thus, it becomes paramount to investigate the effectiveness of the application of such resilience measures in reducing extreme urban heat under future climatic conditions in Porto urban area. This study aims to investigate and quantify the application of urban heat resilience strategies under future climate projections for Porto urban area, using as case study an extreme heat wave that, according to future climate projections downscaled to Porto area, will occur in the medium-term future.

2. Data and methods

2.1. Future climate projections and identification of future heat waves in Porto urban area

IPCC AR5 (2013) includes the latest existent knowledge about the scientific, technical and socio-economic aspects of climate change, and relies on the World Climate Research Programme Fifth Coupled Model Intercomparison Project (CMIP5, details in Taylor et al., 2012), which provides projections of future climate from the present date up to 2100 and beyond. These future climate projections are known as Representative Concentration Pathways (RCP's). In this study, future climate data was taken from RCP 8.5 future climate projection, a "business as usual" scenario characterized by escalating greenhouse gases (GHG) emissions and high concentration levels of these gases in the atmosphere. RCP 8.5 can be seen as the projection of future GHG concentration and radiative forcing if no emissions mitigation strategies are employed until the end of the 21st century. Although more optimistic scenarios are available, this one is usually considered by the scientific community as the most probable, since it is in line with future expectations of GHG emissions. From the wide range of global models available in CMIP5, data from the Max Planck Institute for Meteorology Earth System

Model (MPI-ESM, Giorgetta et al., 2013) was considered in the present work. The overall superiority of MPI-ESM models (as well as their earlier versions) is backed by studies such as Brands et al. (2011, 2013). Marta-Almeida et al. (2016) performed a dynamical downscaling of the MPI-ESM RCP 8.5 global data with the Weather Research and Forecast (WRF) model (Skamarock et al., 2008) to a regional scale (Iberian Peninsula at 9 km of horizontal resolution) for past-present (1986–2005) and future periods (2016–2035, 2046–2065 and 2081–2100). Using this climatic dataset for the medium-term future (2046–2065), future heat waves occurring in Porto urban area were identified following the methodology described in Russo et al. (2014), and the one that showed the highest extreme temperatures was selected as case study for the present work. This methodology defines a heat wave as a 3 consecutive days (or longer) period with the maximum temperature above the daily threshold for the reference period (1981–2010), where this threshold is defined as the 90th percentile of the daily maxima centred on a 31-day window. This heat wave has a duration of 3 days and occurs from 24 to 26 of July 2049, reaching temperatures above 35 °C. The heat wave mean (average of the hourly temperatures) and maximum (average temperatures occurring between 13:00 and 15:00 of each day) surface temperature field of this heat wave, for Porto urban area, is shown in Fig. 1.

2.2. WRF urban modelling system

After the heat wave identification, meteorological data from the regional climatic dataset corresponding to the heat wave days were dynamically downscaled to urban scale with the integrated WRF urban modelling system. WRF and its urban component have been extensively applied in urban areas, particularly in addressing future climate change impacts in urban environments and aiding the development of mitigation and adaptation strategies to cope with extreme meteorological events (Chen et al., 2011, and references therein). This cross-scale atmospheric modelling system provides a realistic coupling between synoptic/mesoscale and urban/local scale meteorology that allows the simulation of meteorological conditions from regional to urban, and even local, scales. WRF urban modelling system consists in a coupling between the WRF atmospheric model and the single layer urban canopy model (SLUCM), available as a WRF module and described in Kusaka et al. (2001) and Kusaka and Kimura (2004). WRF atmospheric model coupling with the SLUCM is made through the Noah land surface model (LSM), responsible for the surface fluxes and temperature of vegetated urban areas, while the SLUCM deals with the anthropogenic and artificial surfaces fluxes. A detailed description of WRF urban modelling system can be found in Chen et al. (2011).

The dynamical downscaling of the meteorological data from the regional climatic dataset to urban scale was performed for a control run and for five different resilience scenarios to analyse the effect of the application of the resilience measures. The only difference between the control run and the five runs with resilience measures is the inclusion of a selected resilience strategy. The characteristics of the resilience runs are detailed in Section 2.2.2, while all other modelling details shared by the resilience and control runs are presented in Section 2.2.1.

2.2.1. Initial and boundary conditions, simulations domain and design

As aforementioned, the initial and boundary data for the heat wave simulations were extracted from the regional climatic dataset of Marta-Almeida et al. (2016). A multiple nesting strategy was followed to downscale this meteorological data to Porto urban area. The innermost simulation domain, with 200 m of horizontal resolution, is depicted in Fig. 2.

Topography data from the Shuttle Radar Topography Mission (SRTM) project (Farr et al., 2007) with 3 arc-seconds of horizontal resolution (approx. 100 m for the region under study) was used to represent the topography in the simulation domain. Information regarding the land use/land cover was taken from the Corine land cover project (Büttner et al., 2000) 2006 version (CLC2006), also with 3 arc-seconds of horizontal resolution. In addition to CLC2006, also land use/land cover high-resolution data (10×10 m) from the European Environmental Agency Porto Urban Atlas (available in http://www.eea.europa.eu/data-and-maps/data/urban-atlas) was used to better detail Porto urban features. CLC2006 and Porto Urban Atlas land use datasets were remapped to the United States Geological Survey (USGS) 33 land use categories, which considers 3 different urban categories: the High Intensity Residential includes highly developed areas where people reside in high numbers (apartment complexes, row houses, etc.); the Low Intensity Residential includes areas with a mixture of constructed materials and vegetation where population densities are lower than in high intensity residential areas (single-family housing units, etc.); and Industrial/Commercial, which includes

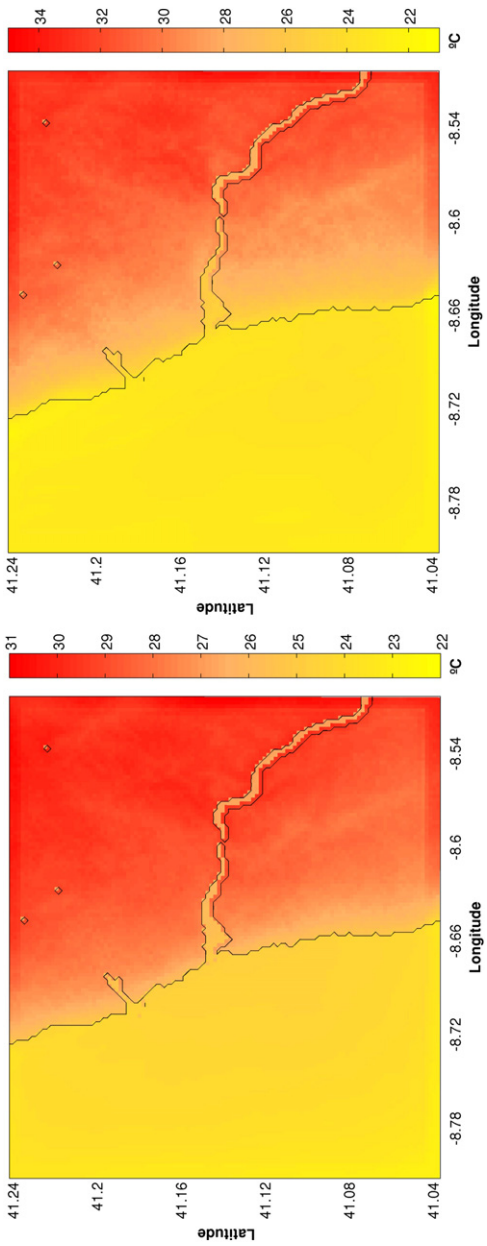

Fig. 1. Mean (left) and maximum (right) temperature fields for the selected heat wave.

Fig. 2. Innermost simulation domain (1 cm:30 km).

infrastructures (roads, railroads, airports, harbours, etc.) and all other built areas that do not fit into the residential categories. The remapping of CLC2006 to USGS 33 land use categories followed the methodology proposed by Pineda et al. (2004), with the exception of the urban green areas: Pineda et al. (2004) included this category (CLC2006 land use category 10, urban green areas) in the USGS category of Industrial/Commercial (USGS land use category 33). For the present work, this CLC2006 land use category 10 (green urban areas) was remapped to the USGS land use category 3 (Irrigated Cropland and Pasture), in order to represent green urban areas as vegetated areas and not as built areas. Table 1 summarizes the CLC2006 44 land use categories conversion to USGS 33 categories. Table 2 details and proposes a conversion methodology for the remapping of European Environmental Agency Porto Urban Atlas to USGS land use categories methodology, given the lack of references on this subject. CLC2006 and Porto Urban Atlas data were combined in a complementary strategy: Porto Urban Atlas data was used for the domain areas where it is available, while CLC2006 for areas where such data was not.

Besides the aforementioned use of the Noah LSM parameterization scheme, the physical configuration shared by all simulations considered the following sub-grid parameterization options: Yonsei University for the planetary boundary layer, Monin-Obukhov for the surface layer, Double-Moment 6-Class for the microphysics, RRTMG scheme for the long-wave and short-wave radiation. Since the horizontal resolution of all simulations is 200 m no cumulus parameterization was employed it, being assumed that vertical fluxes due to updrafts and downdrafts and compensating motion outside the clouds can be resolved explicitly at grid sizes of approximately 5–10 km or lower (Skamarock et al., 2008). It could also be argued that at such sub-kilometre horizontal resolutions no PBL parameterizations should be used since at these scales the smallest resolvable scale is comparable to the large eddy scales in the convective boundary layer (Shin and Dudhia, 2016). However, at such high-resolution, sub-kilometre scales, grid sizes fall within a “terra incognita” or “grey zone” (as previously reported by several studies such as Shin and Dudhia, 2016; Wyngaard, 2004; Zhou et al., 2014), and no consensus is established whether a PBL parameterization should be used or not.

The simulation results here presented, which used a PBL parameterization, appear realistic and robust in the way that no significant unphysical or spurious circulations were detected in the near surface temperature, winds and relative humidity fields.

To better represent the sub-grid scale variability in land use/land cover composition, the Noah LSM was used with the sub-tiling option (described in detail in Li et al. (2013)). The SLUCM options to consider urban irrigation, anthropogenic heating added to latent heat flux term and evaporation over impervious surface were also used. A detailed description of these options can be found in Yang et al. (2015). Fig. 3 illustrates and summarizes the modelling chain followed in this study.

2.2.2. Resilience scenarios

As aforementioned, three different resilience factors were applied to Porto urban area and their ability to reduce extreme urban temperatures occurring during the selected heat wave was analysed and quantified. The resilience factors consisted in the application of green roofs, white roofs and the increase of Porto green urban areas. Five different resilience scenarios were built using these three resilience factors:

The scenario **S1** considered an increase of Porto green urban area to an area that duplicates its present extension. For that, a new simulation domain was built where the number of grid points that originally had an USGS land use category of "green urban area" in the control run simulation domain were duplicated, this is, the land use category was changed from its original value to the USGS land use category 3. This scenario mimics the increase of Porto urban green area to a size that, approximately, duplicates its current area, as it can be seen in Fig. 4.

Scenario **S2** simulates the application of green roofs (covered with vegetated surfaces) in 75% of the urban areas, this is, the simulation grid cells with USGS land use urban categories (31, 32 and 33). It should be noted that since the SLUCM considers a spatial average of each urban grid cell, no distinction is made among individual buildings within each urban grid cell (Li et al., 2014). Thus, this fraction of green roofs can be considered as either 75% of buildings within the grid cell are covered by green roofs while 25% of the buildings are covered by conventional roofs, or each building is covered by 75% of green roofs and 25% of conventional roofs. The green roof system integrated in WRF SLUCM is detailed in Yang et al. (2015). When compared to a conventional roof, it has three additional layers on the top: vegetation, soil and growing media layers. Scenario **S3** simulates the application of white roofs (roofs painted white or covered with white materials) in an area with equivalent extension of the area in which were simulated the application of green roofs (scenario S2). Since approximately 75% of the urban cells belong to the USGS category of 31 and 33 (commercial and low-intensity residential area), white roofs application was simulated in the grid cells defined as commercial and low-intensity residential areas. For these grid cells, the roof surface albedo was defined as 80%, following the values proposed by Susca (2012) for the albedo of a white-colour newly painted roof. This way, the number of grid cells of the simulation domain in which were tested the application of green and white roofs are approximately the same, making the simulation results directly comparable for these resilience scenarios. It should be noted that this was not the case for scenario S1, due to the unrealistic case that 75% of a given (real) urban area would be converted to green areas. Scenario **S4** simulates the simultaneous application of scenarios S1 and S2 (increase of the urban green areas and application of green roofs), while scenario **S5** simulates the simultaneous application of scenarios S1 and S3 (increase of the urban green areas and application of white roofs).

As previously described, the control and resilience scenarios were run for the heat wave period (24–26 July 2049) for Porto urban area. Besides the selected heat wave, other four heat waves were identified (following the methodology proposed by Russo et al., 2014) and considered as test case studies. The same control and resilience scenarios were run for these additional 4 heat waves to confirm the consistency of the results obtained for the 24–26 July 2049 heat wave. Since the results for these additional 4 heat waves were similar to the results obtained for the selected heat wave (24–26 July 2049), only the results of this heat wave are presented. Nevertheless, the validity of such results is strongly backed by other 4 case studies.

3. Results and discussion

This section presents the simulation results for the selected future heat wave in Porto urban area. The effects of the resilience factors application (scenarios S1 to S5) on the surface temperature and relative humidity

Table 1
Corine land cover 2006 (CLC2006) 44 categories equivalence to USGS 33 land use categories.

Corine land cover 2006 (CLC2006)		Corine land cover 2006 (CLC2006) – USGS Equivalence													
CLC2006 land use category	Nomenclature	USGS land use category	Nomenclature	Albedo (%)		Surface moisture availability (%)		Surface emissivity (% at 9 μm)		Surface roughness length (cm)		Surface thermal inertia ($cal \cdot cm^{-2} \cdot K^{-1} \cdot s^{-1/2}$)		Soil heat capacity ($J \cdot m^{-3} \cdot K^{-1}$)	
				W	S	W	S	W	S	W	S	W	S	W	S
1	Continuous urban fabric	32	High intensity residential	10	10	10	10	97	97	80	80	0.3	0.3	1.67	1.67
2	Discontinuous urban fabric	31	Low intensity residential	10	10	10	10	97	97	80	80	0.3	0.3	1.67	1.67
3	Industrial or commercial units	33	Industrial/commercial	10	10	10	10	97	97	80	80	0.3	0.3	1.67	1.67
4	Road and rail networks and associated land														
5	Port areas														
6	Airports														
7	Mineral extraction sites														
8	Dump sites														
9	Construction sites														
11	Sport and leisure facilities														
12	Non-irrigated arable land	2	Dryland cropland and pasture	20	17	60	30	92	98.5	5	15	0.4	0.4	2.00	2.71
18	Pastures														
10	Green urban areas	3	Irrigated cropland and pasture	20	18	50	50	93	98.5	20	10	0.4	0.4	1.76	2.20
13	Permanently irrigated land														
14	Rice fields														
15	Vineyards	6	Cropland/woodland mosaic	20	16	60	35	93	98.5	20	20	0.4	0.4	2.00	3.19
16	Fruit trees and berry plantations														
17	Olive groves														
19	Annual crops associated with														

	permanent crops														
20	Complex cultivation patterns														
21	Land principally occupied by agriculture, with significant areas of natural vegetation														
22	Agro-forestry areas														
26	Natural grasslands	7	Grassland	23	19	30	15	92	96	10	12	0.4	0.3	2.00	2.37
27	Moors and heathland	9	Mixed shrubland/grassland	22	20	25	15	93	95	10	60	0.4	0.3	1.24	2.14
28	Sclerophyllous vegetation														
29	Transitional woodland-shrub														
23	Broad-leaved forest	11	Deciduous broadleaf forest	17	16	60	30	93	93	50	50	0.5	0.4	2.40	2.63
24	Coniferous forest	14	Evergreen needleleaf forest	12	12	60	30	95	95	50	50	0.5	0.4	3.00	3.33
25	Mixed forest	15	Mixed forest	14	13	60	30	93	97	20	50	0.6	0.4	1.12	2.11
40	Water courses	16	Water bodies	80	80	10	10	98	98	10	10	0.6	0.6	0.00	0.00
41	Water bodies														
42	Coastal lagoons														
43	Estuaries														
44	Sea and ocean														
35	Inland marshes	17	Herbaceous wetland	14	14	75	60	95	95	20	20	0.6	0.6	1.50	1.50
36	Peat bogs														
37	Salt marshes														
38	Salines														
39	Intertidal flats														
30	Beaches, dunes and sand	19	Barren or sparsely vegetated	23	25	50	20	90	90	10	10	0.2	0.2	0.81	0.81
31	Bare rocks														
32	Sparsely vegetated areas														
33	Burnt areas														
34	Glaciers and perpetual snow	24	Snow or ice	70	55	95	95	95	95	10	10	0.5	0.5	0.00	0.00

Table 2
EEA Porto Urban Atlas land cover categories equivalence to USGS land use categories.

EEA Porto Urban Atlas		EEA Porto urban Atlas – USGS equivalence													
EEA land use category	Nomenclature	USGS land use category	Nomenclature	Albedo (%)		Surface moisture availability (%)		Surface emissivity (% at 9 μm)		Surface roughness length (cm)		Surface thermal inertia ($cal \cdot cm^{-2} \cdot K^{-1} \cdot s^{-1/2}$)		Soil heat capacity ($J \cdot m^{-3} \cdot K^{-1}$)	
				W	S	W	S	W	S	W	S	W	S	W	S
11,100	Continuous Urban Fabric	32	High intensity residential	10	10	10	10	97	97	80	80	0.3	0.3	1.67	1.67
11,210	Discontinuous Dense Urban Fabric	31	Low intensity residential	10	10	10	10	97	97	80	80	0.3	0.3	1.67	1.67
11,220	Discontinuous medium density urban fabric														
11,230	Discontinuous low density urban fabric														
11,240	Discontinuous very low density urban fabric														
11,300	Isolated structures	33	Industrial/commercial	10	10	10	10	97	97	80	80	0.3	0.3	1.67	1.67
12,100	Industrial, commercial, public, military and private units														
12,210	Fast transit roads and associated land														
12,220	Other roads and associated land														
12,230	Railways and associated land														
12,300	Port areas														
12,400	Airports														
13,100	Mineral extraction and dump sites														
13,300	Construction sites														
13,400	Land without current use														
14,200	Sports and leisure facilities														
14,100	Green urban areas	3	Irrigated cropland and pasture	20	18	50	50	93	98.5	20	10	0.4	0.4	1.76	2.2
20,000	Agricultural areas, semi-natural areas and wetlands	6	Cropland/woodland mosaic	20	16	60	35	93	98.5	20	20	0.4	0.4	2.00	3.19
30,000	Forest	15	Mixed forest	14	13	60	30	93	97	20	50	0.6	0.4	1.12	2.11
50,000	Water	16	Water bodies	8	8	10	10	98	98	10	10	0.6	0.6	0.00	0.00

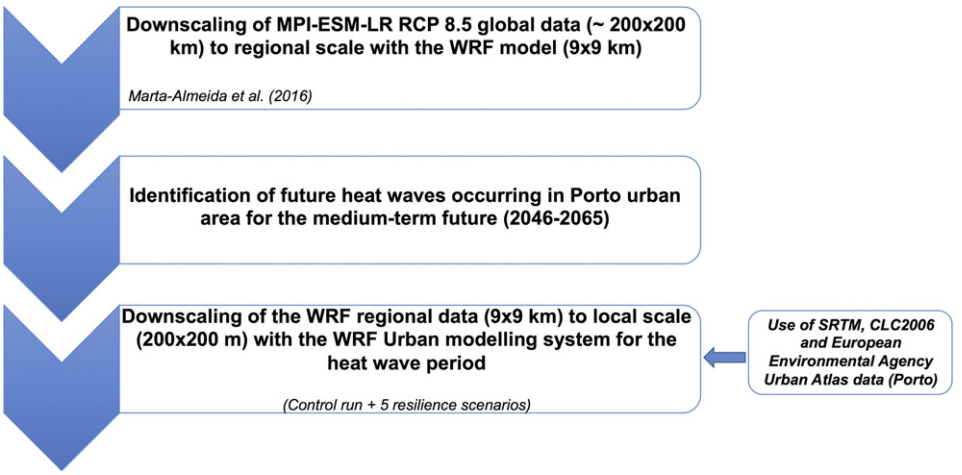

Fig. 3. Modelling flowchart.

fields (defined at a height of 2 m) were investigated, considering the control run (run without resilience factors) as reference.

Differences in the mean (average of the hourly temperatures for the duration of the heat wave), maximum (average temperatures occurring between 13:00 and 15:00 of each day of the heat wave) and nocturnal (average temperatures occurring between 22:00 and 08:00 of each day of the heat wave) surface temperature fields were analysed. Nighttime temperatures also have the potential to affect the urban population thermal comfort, particularly during a heat wave since the quality and quantity of sleep depends heavily on the ambient temperature. Moreover, the buildings ability to cool down in the night through passive cooling will strongly depend if the nighttime temperatures are lower.

Another factor that can impact the urban population comfort is the relative humidity conditions, since the perceived temperature by humans is largely dependent upon the surrounding atmospheric moisture content (Persinger, 1980). Humidity content impacts the body's ability to cool itself by evaporation of perspiration, and under high temperature conditions a high humidity content can diminish the body's ability to evaporate perspiration, leading to heat stress. Considering that all of the resilience scenarios have the potential to cause a humidity increase due to evapotranspiration or temperature decrease (for the same absolute humidity, a lower temperature yields a higher relative humidity), it becomes pertinent to analyse if the resilience scenarios produce a significant increase of the relative humidity, which can counterbalance (partly or totally) their beneficial effect in lowering the temperatures. To this end, differences in the mean surface (2 m) relative humidity between the control and the resilience scenarios were also analysed.

3.1. Resilience scenario S1

Fig. 5 shows that the resilience scenario S1 is able to reduce the mean and maximum temperatures due to an increase in the surface moisture availability and a local cooling caused by evapotranspiration and shading. The reduction in the maximum temperature field is more pronounced than the one seen for the mean temperature field, reaching values of 1 °C. However, the mean and maximum temperature differences show a very localized pattern, being mostly concentrated near the added green urban areas. It is also visible in the maximum temperature difference fields that this resilience scenario induces a very localized slight increase of the maximum temperature in the parks neighbouring area. This is due to the existence of a pressure gradient between the green area and the built-up surroundings that produce a convergence of warmer air above the park (Oke et al., 1989).

Another pressure gradient, resulting from the land use and temperature differences between the green areas (cooler) and its built-up surroundings (warmer), will lead to a cooler air advection from the green areas to the built-up surroundings. This effect is known as the park breeze effect (Oke et al., 1989) or park

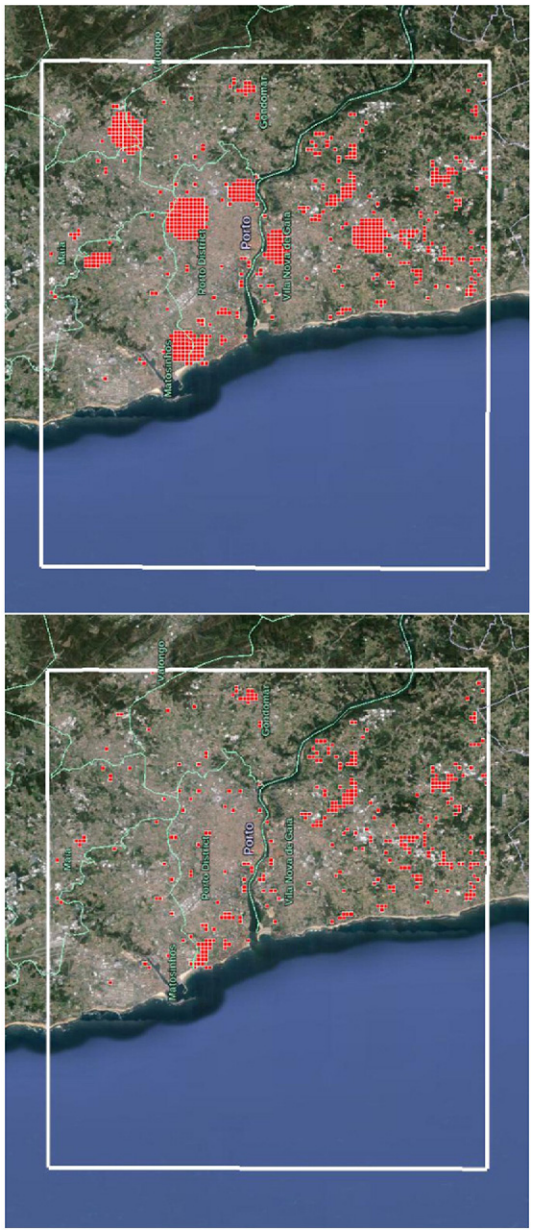

Fig. 4. Control run USGS land use category 3 grid cells (left) and S1 run USGS land use category 3 grid cells (right).

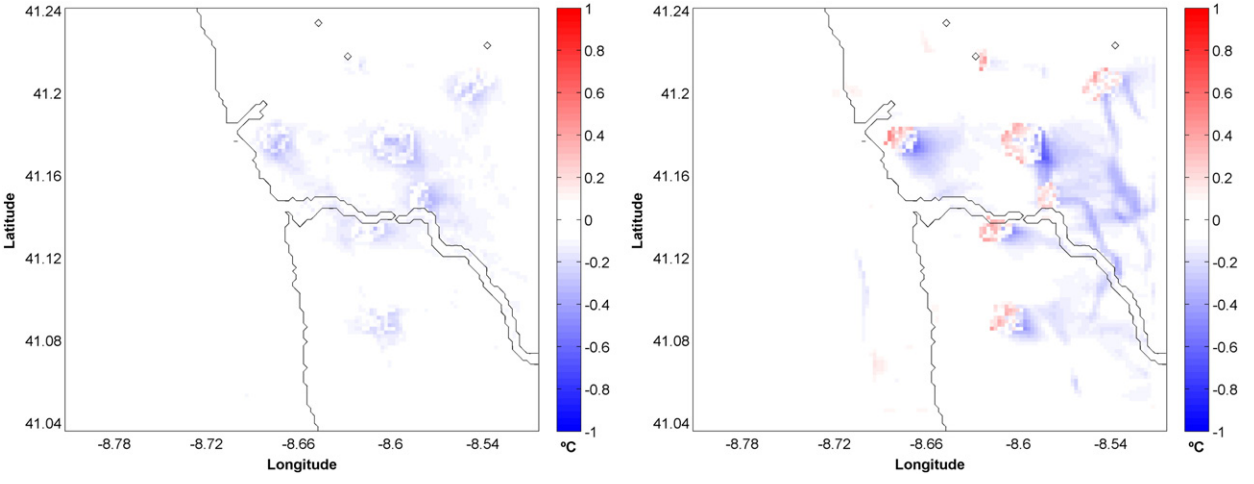

Fig. 5. Mean (left) and maximum (right) temperature difference fields (S1-control run) for the future heat wave.

cool islands (Spronken-Smith and Oke, 1998). In Fig. 5 it is clear the advection of cooler air to Southeast of the added green areas: in summer periods, the typical atmospheric circulation in the North Atlantic coastal areas of Portugal is southward, particularly during daytime and early afternoon. Moreover, in such periods the formation and development of sea breezes (wind coming from the sea to inland areas) is quite common, and the lower friction/surface roughness of the green areas will enhance the sea breeze influence and inland extent (Papangelis et al., 2012). The interaction between the synoptic southward winds and the mesoscale sea breezes blowing eastward will originate the South-eastward transport of cooler air masses from the green urban areas to their surroundings.

Fig. 6 shows the temperature differences between the scenario S1 and the control run for nighttime periods.

The resilience scenario S1 also produces a cooling effect in nighttime periods, albeit less pronounced than the one seen for daytime. The fact that this resilience scenario was able to reduce the temperature during the day (shading and evapotranspiration) impacts positively the nocturnal temperature field. The temperature reduction is typically around 0.3–0.5 °C and, similarly to what was seen for daytime, this cooling effect is more pronounced in the vicinity of the added green areas. This cooling effect will allow a more efficient passive cooling of the buildings, contributing to an increase of the citizen's thermal comfort and allowing a relief from the daytime higher temperatures.

Fig. 7 shows the relative humidity differences between scenario S1 and the control run (mean differences for the heat wave duration).

As expected, an increase of urban green areas induces an increase of the relative humidity, since evapotranspiration releases moisture to the surrounding areas. These differences are, however, limited to the vicinity of the added green areas and are relatively low, never going beyond a 2–3% relative humidity increase. This modest increase in the RH field is not expected to negatively impact the population thermal comfort.

3.2. Resilience scenario S2

Fig. 8 shows that the resilience scenario S2 (application of green roofing) clearly reduces urban temperatures. The mean temperatures are reduced around 0.5 °C, while the maximum temperatures decreased up to

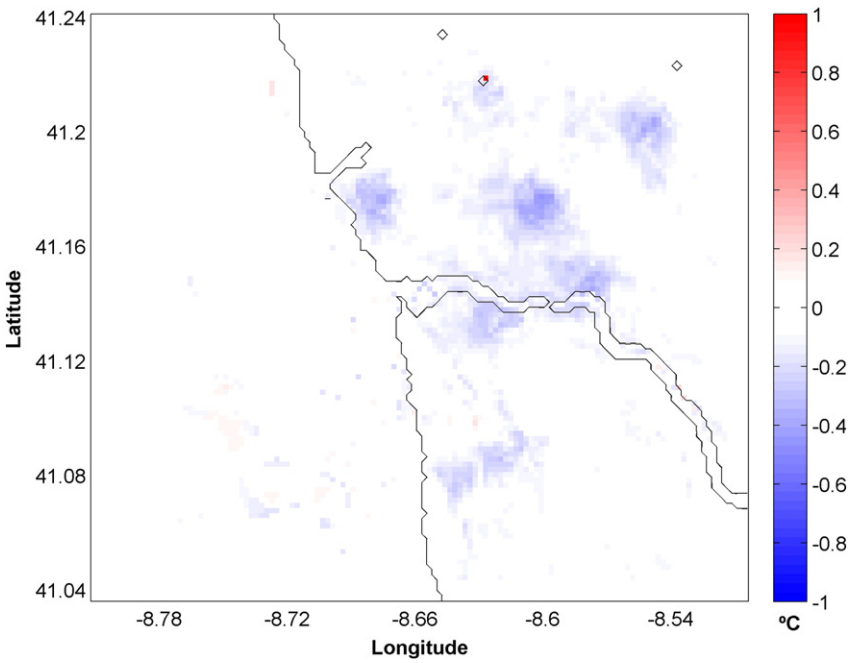

Fig. 6. Nocturnal temperature difference fields (S1-control run) for the future heat wave.

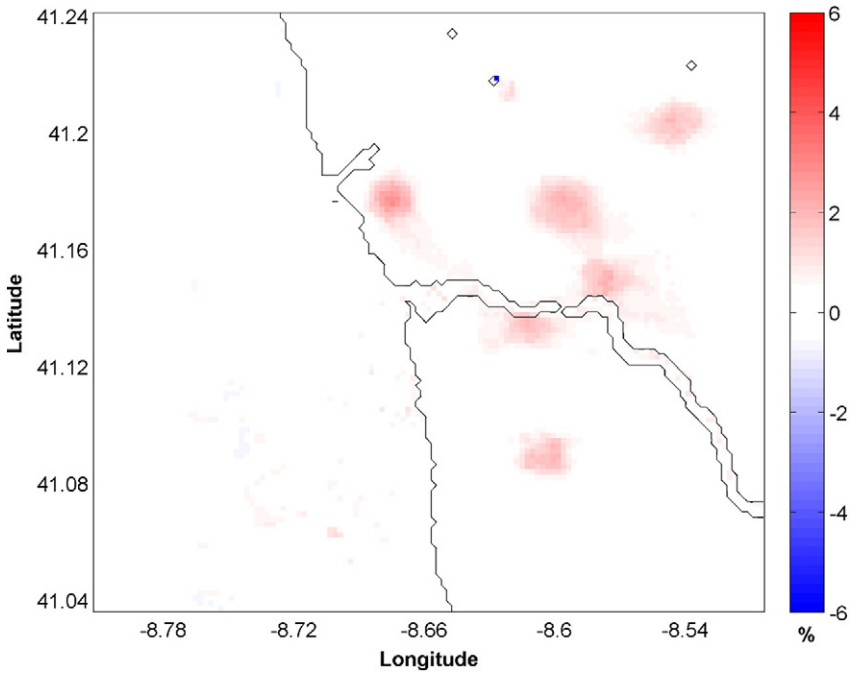

Fig. 7. Relative humidity difference fields (S1-control run) for the future heat wave.

1 °C. Since green roofs were evenly applied across the urban area, the resulting temperature reduction is also practically uniform throughout the urban area. Similarly to what was seen in Fig. 5 for the resilience scenario S1, a green roof surface temperature is significantly lower than the one of a conventional roof due to the increase in the surface moisture availability, evapotranspiration and shading provided by the green roof vegetated surface. Although not shown in this study, several other runs were made with increasing percentages of green roof application (25, 50 and 75%, the one shown here), and it was clear that increasing green roof coverage increasingly reduced the surface temperatures.

Fig. 9 shows the temperature differences between the scenario S2 and the control run for nighttime periods.

Although the relatively strong temperature reduction achieved by this resilience scenario seen in Fig. 8, for nighttime periods the application of scenario S2 does not produce a relevant temperature reduction. While some areas show a temperature reduction, other areas witness a temperature increase. However, these differences can be regarded as residual since they never surpass 0.1–0.2 °C. Given that green roofs are usually lightly vegetated surfaces (small shrubs, flowers or bushes) when compared to urban parks (usually contain trees and denser vegetation), their ability to reduce nighttime temperatures is lower.

Fig. 10 shows the relative humidity differences between the scenario S2 and the control run (mean differences for the heat wave duration), where it is visible a slight increase of the RH (order of 2–3%). This higher RH mean field can be explained by the combined effect of the surface moisture release originated by the added vegetated surfaces evapotranspiration and the reduction of the temperature field (Fig. 8): an increase of the surface moisture means higher absolute humidity that, associated with lower temperatures, will enhance and further increase the relative humidity. Again, these differences are rather small in magnitude, and don't seem to be able to cause discomfort to the urban population.

3.3. Resilience scenario S3

According to Fig. 11, the resilience scenario S3 (application of white roofs) shows an ability to reduce urban temperatures similar to the green roofing option (S2), although the latter seems to show a stronger

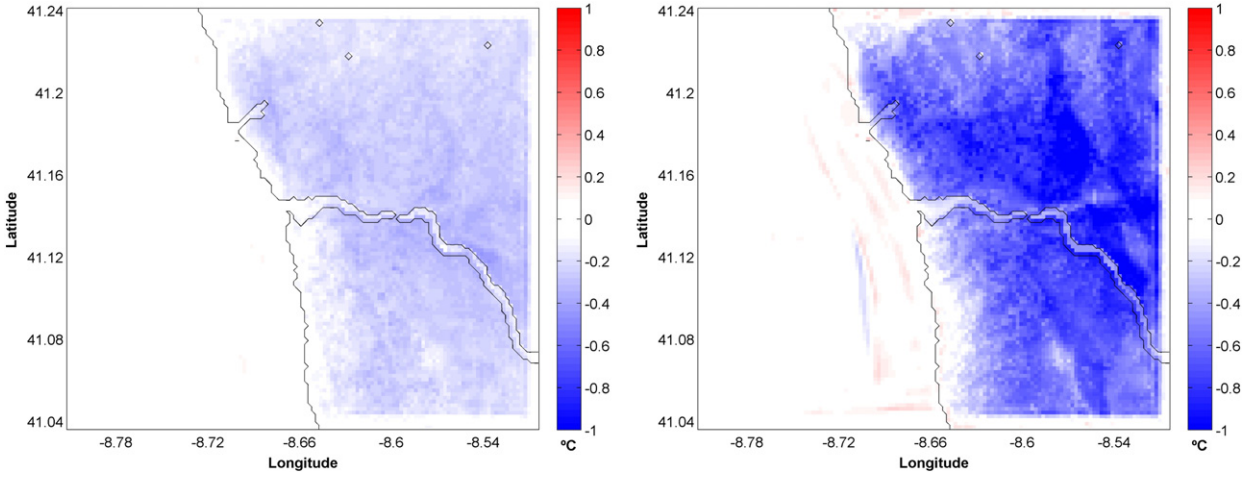

Fig. 8. Mean (left) and maximum (right) temperature difference fields (S2-control run) for the future heat wave.

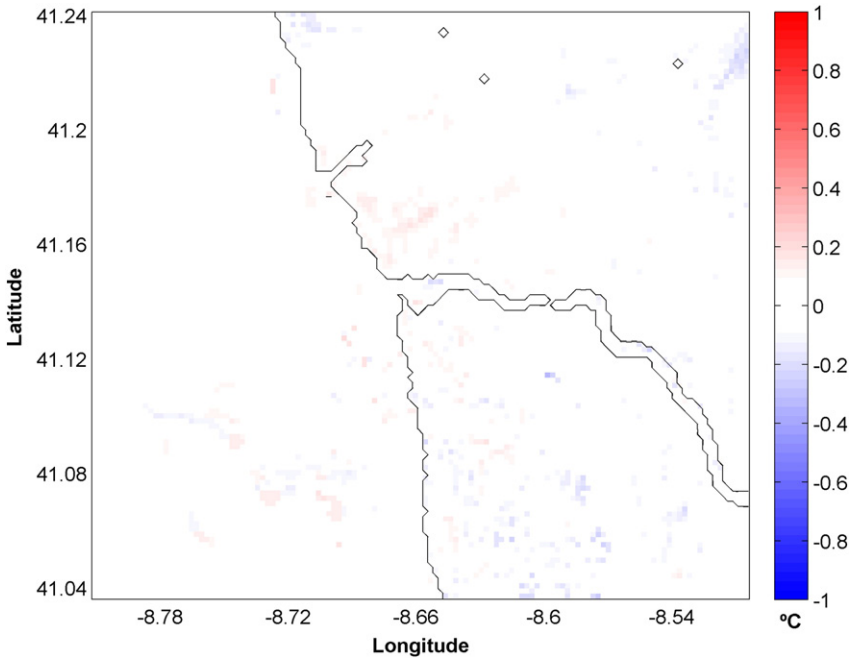

Fig. 9. Nocturnal temperature difference fields (S2-control run) for the future heat wave.

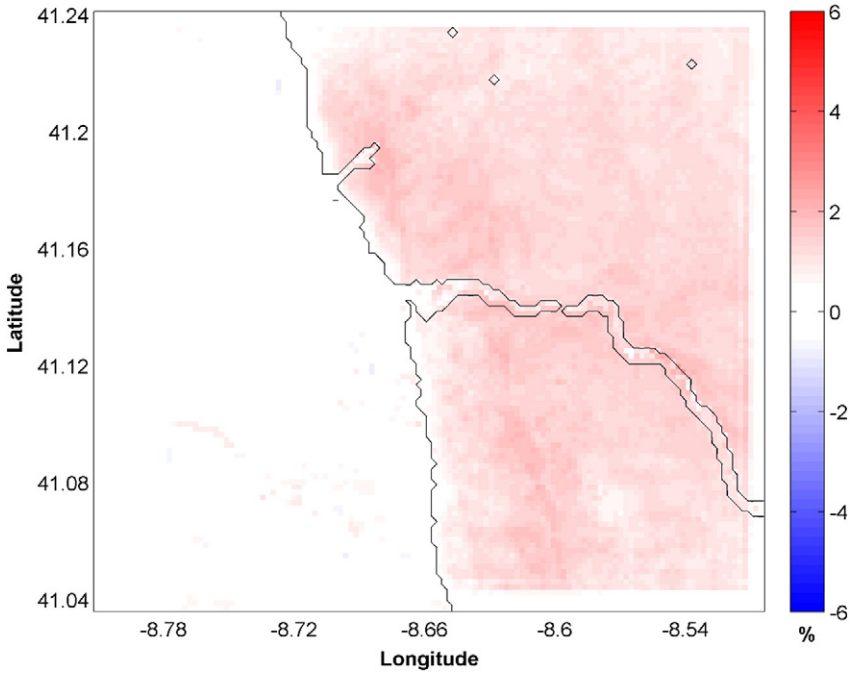

Fig. 10. Relative humidity difference fields (S2-control run) for the future heat wave.

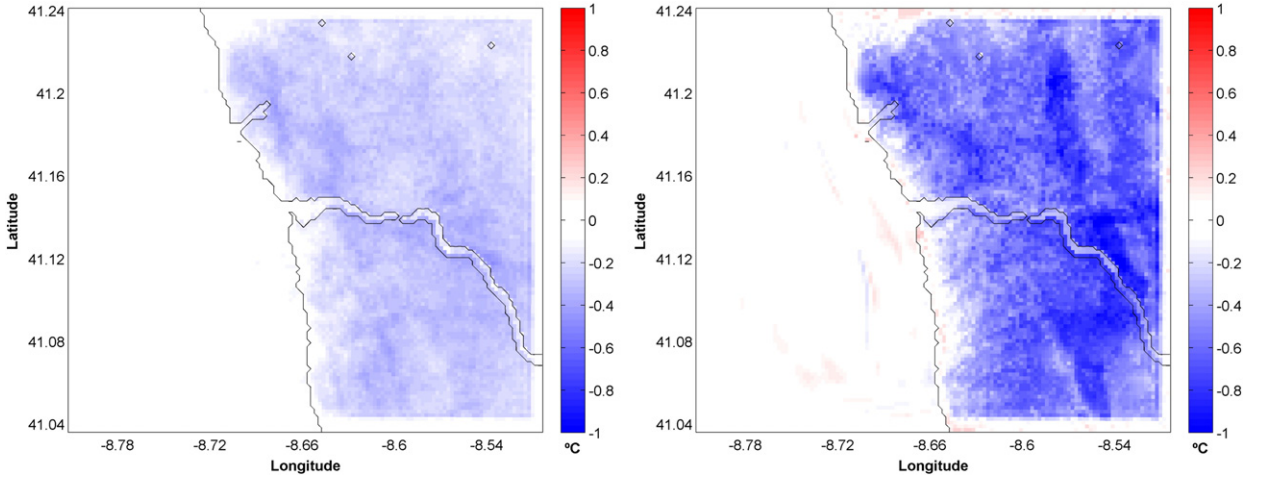

Fig. 11. Mean (left) and maximum (right) temperature difference fields (S3-control run) for the future heat wave.

ability to reduce the maximum temperature field. The typical temperature reduction achieved by this resilience scenario is of about 0.4–0.6 °C for the mean temperature, reaching 1 °C in the maximum temperature field. The geographical distribution of the temperature differences is coherent with the location of the commercial and low-intensity residential grid cells, where the albedo increase was changed to 80% to mimic the application of white roofs. The white roofs properties (thermal and others) are the same as the ones of conventional roofs, with the exception of their surface albedo. Taking into account that the white roofs albedo is much higher than the albedo of green roofing, Figs. 5, 8 and 11 show that the effects of shading, evapotranspiration and increase in the surface moisture availability produced by green roofs (and also increase of green areas, although in this case the impacts are very localized) are able to offer a significant contribution to lowering urban temperatures, producing the same quantitative results as the application of a surface with a much higher albedo.

Fig. 12 shows the temperature differences between the scenario S3 and the control run for nighttime periods.

Oppositely to what was seen for the green roofs option (S2), the application of white roofs is able to produce an interesting nocturnal temperature reduction, reaching values of around 0.5 °C. This can be explained by the fact that, if the buildings and paved surfaces are coated with higher albedo materials, they will accumulate lower amounts of heat during the day. Thus, their temperature will also be lower in nigh periods. Also, by applying this resilience measure, no temperature increase is seen due to evapotranspiration. Next, Fig. 13 shows the relative humidity differences between the S3 resilience scenario and the control run.

Similarly to what was seen for scenario S2, this resilience strategy produces a slight increase in the mean RH field, although lower than the one seen for scenario S2 (scenario S3 does not produce evapotranspiration that contributes for the increase of the RH field). This increase in the RH can be explained by the lower urban temperatures produced by this resilience scenario. Nevertheless, the RH increase does not seem to surpass 1–2%, not enough to impact the population thermal comfort.

3.4. Resilience scenario S4

Fig. 14 shows that the combined application of resilience scenarios (S4) corresponds almost linearly to the sum of each resilience scenarios application (S1 and S2) effects. The temperature reduction achieved by S4 is

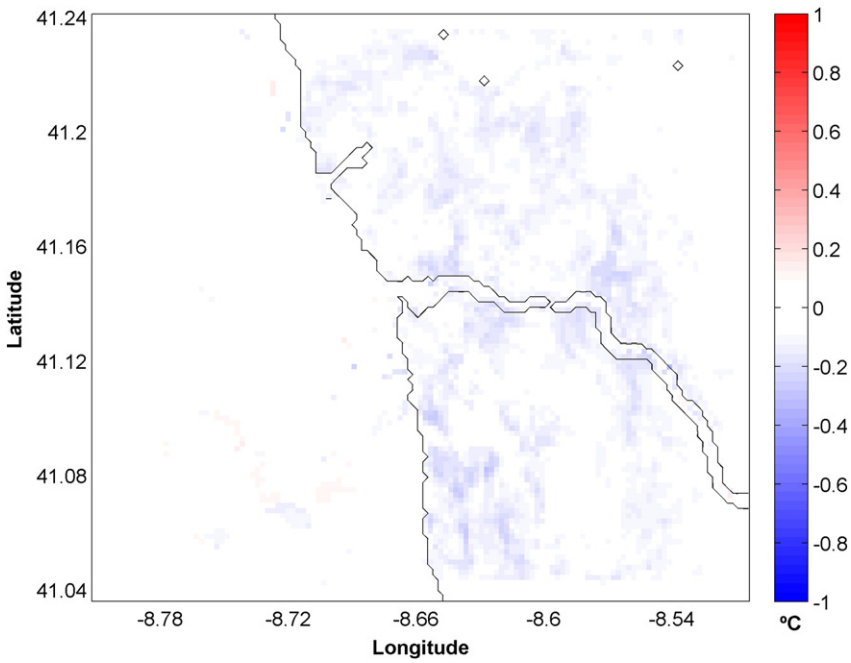

Fig. 12. Nocturnal temperature difference fields (S3-control run) for the future heat wave.

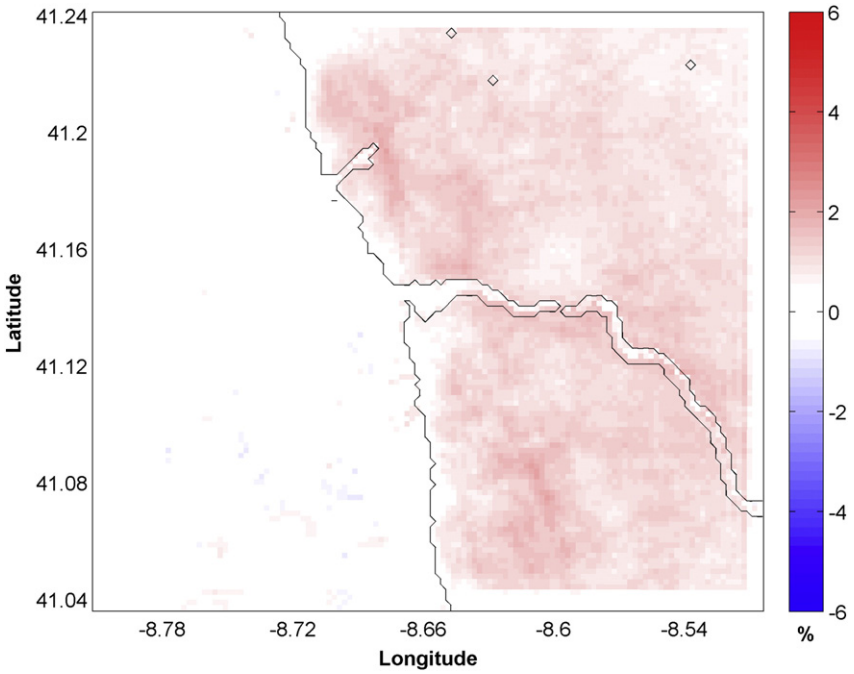

Fig. 13. Relative humidity difference fields (S3-control run) for the future heat wave.

significant, with an average temperature reduction of 0.5 °C (for the mean) and 1 °C (for the maximum) for almost all the simulation domain. The park breeze/park cool island effect is also present in this case, although the green roofs effect clearly masks the individual effect of the added green urban areas. Fig. 15 depicts the nighttime surface temperature field differences when the resilience scenario S4 is applied.

Fig. 15 shows an interesting factor. The nocturnal temperature reduction achieved by this scenario seems to be higher than the combined and cumulative effect of applying S1 and S2. This might indicate the existence of non-linear interactions between the application of green roofing and the presence of urban parks that might enhance their individual effects and achieve higher performances in reducing nocturnal urban temperatures. Next, Fig. 16 shows the relative humidity field differences between the scenario S4 and the control run.

Fig. 16 confirms that the effect of applying the resilience strategy S4 is mainly a cumulative effect of applying the resilience strategies S1 and S2. An increase of the relative humidity is seen in almost all Porto urban area, with localized areas of higher relative humidity increase that coincide with the locations of the added green areas (higher evapotranspiration than the green roofs). Even so, these relative humidity increase are limited to about 2–3%, not enough to significantly affect the population thermal comfort.

3.5. Resilience scenario S5

Figs. 17 to 19 reveal that the combined application of two resilience measures (S5) produces a combined effect that practically matches the sum of the individual effects of each resilience scenarios application (S1 and S3). The combined application of S1 and S3 produces a mean temperature reduction very similar of the one obtained with the combined application of S1 and S2 (S4), although the latter is able to reduce more the maximum temperature field. Oppositely, the application of S5 shows a more widespread reduction of the nighttime temperatures, given the white roofs higher effectiveness in lowering nocturnal temperatures when compared to green roofs (Fig. 9 vs. Fig. 12). Similarly to what was seen in Fig. 15 for scenario S4, Fig. 18 shows that the nocturnal temperature reduction achieved by S5 seems higher than the cumulative effect of applying S1 and S3, possibly a sign of non-linear interactions between the application of white roofs and the presence of urban parks that enhance their independent effects and achieve higher performances in

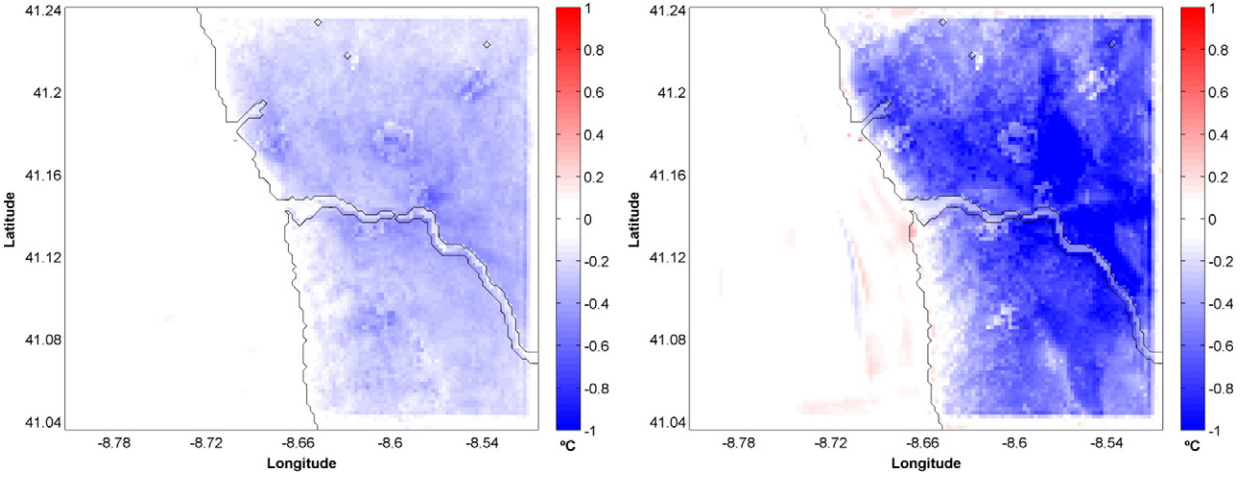

Fig. 14. Mean (left) and maximum (right) temperature difference fields (S4-control run) for the future heat wave.

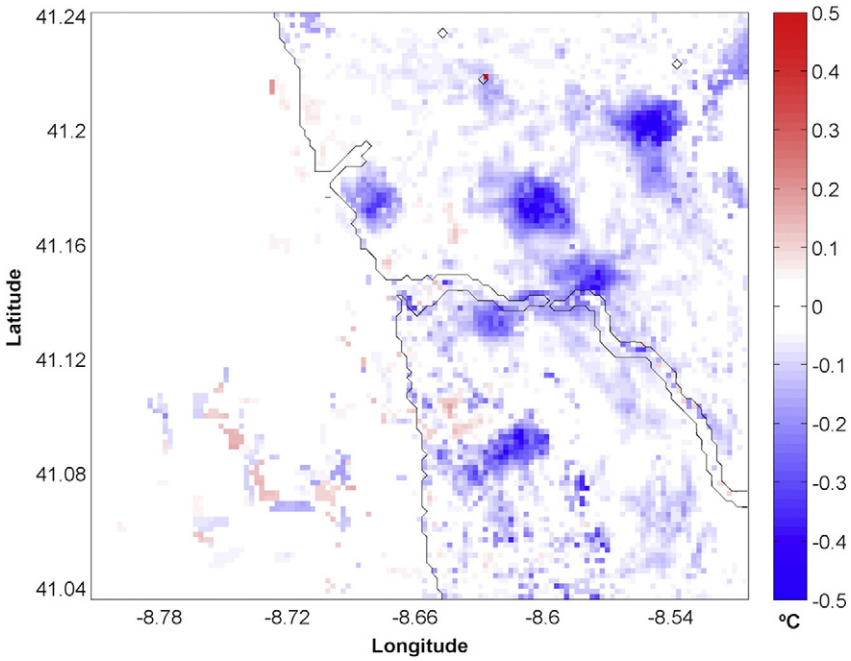

Fig. 15. Nocturnal temperature difference fields (S4-control run) for the future heat wave.

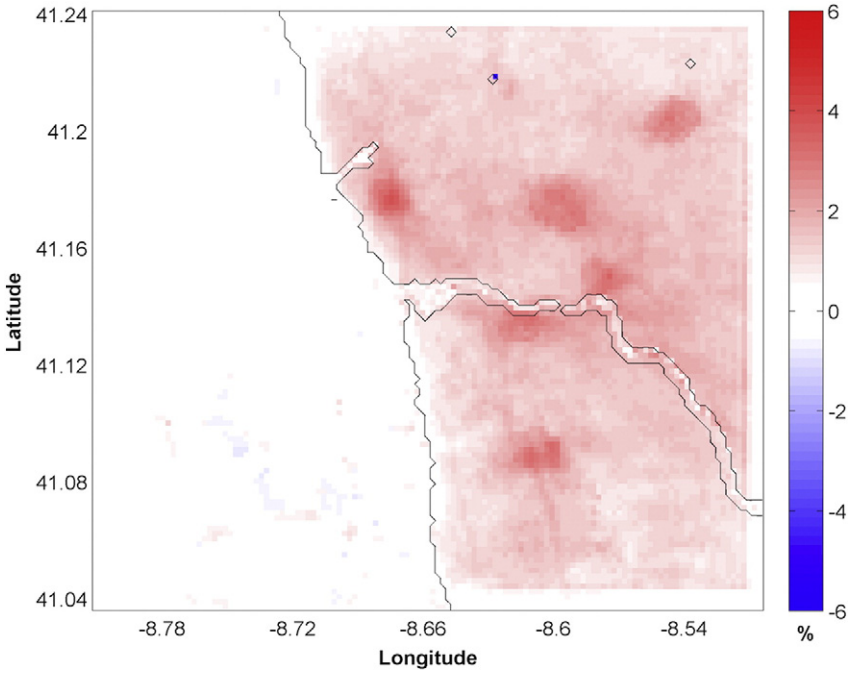

Fig. 16. Relative humidity difference fields (S4-control run) for the future heat wave.

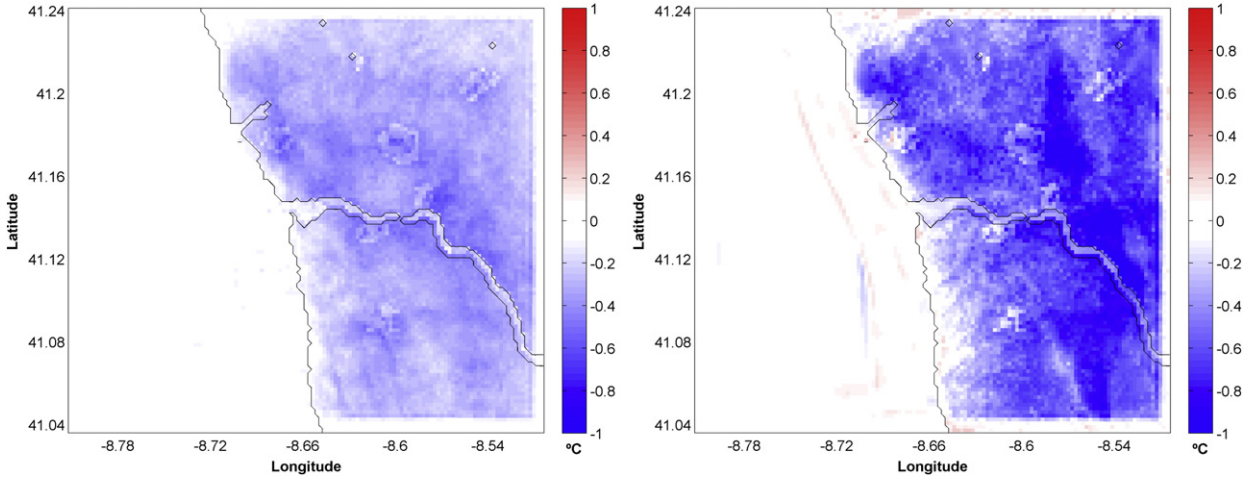

Fig. 17. Mean (left) and maximum (right) temperature difference fields (S5-control run) for the future heat wave.

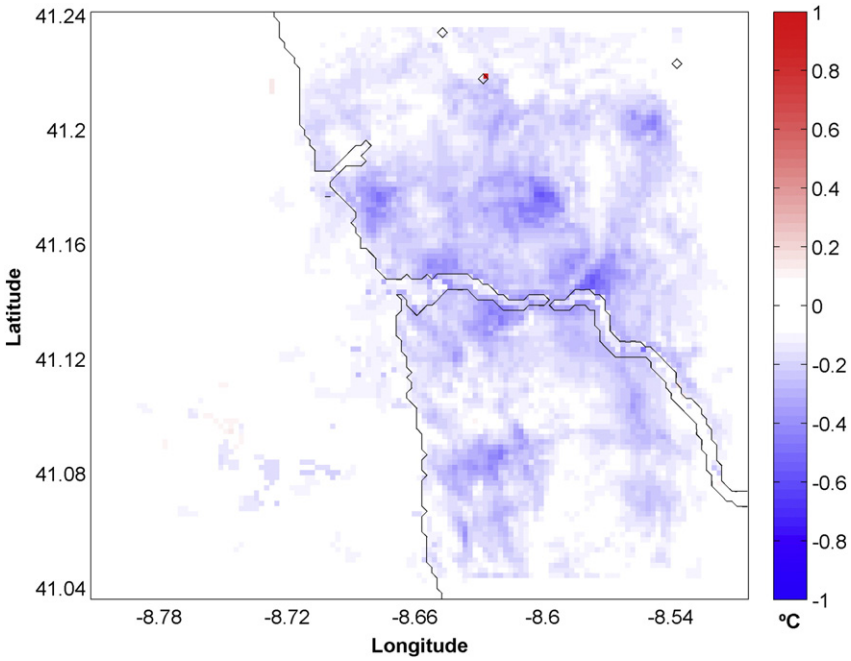

Fig. 18. Nocturnal temperature difference fields (S5-control run) for the future heat wave.

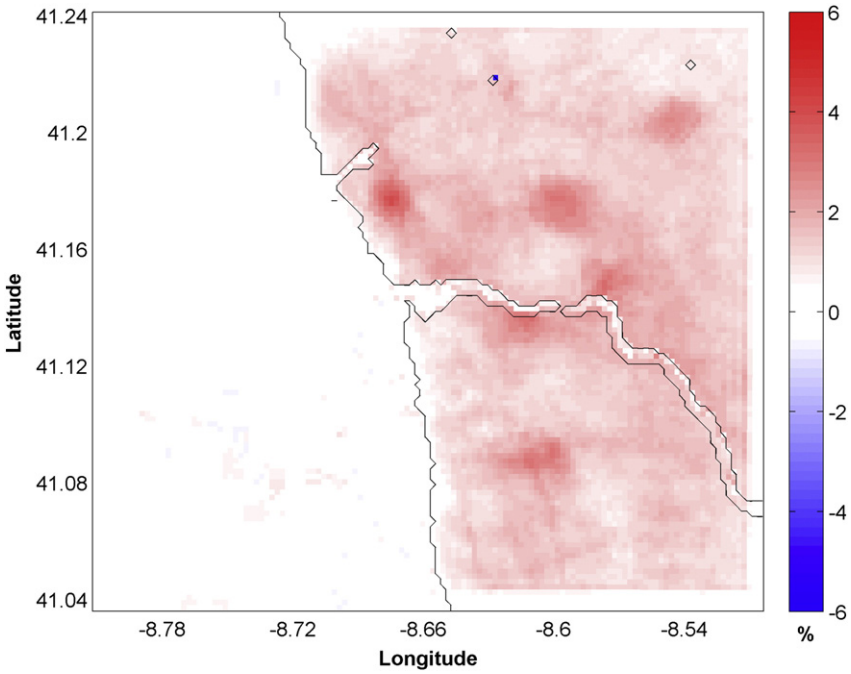

Fig. 19. Relative humidity difference fields (S5-control run) for the future heat wave.

reducing nocturnal urban temperatures. Fig. 19 also shows a cumulative effect in the relative humidity increase produced by the combination of scenarios S1 and S3. Although higher than the independent effect of each one of these resilience scenarios, this increase (typically below 2–3%) is not expected to significantly affect the thermal confront of the urban population.

Figs. 5 to 19 show that albeit all the tested resilience scenarios are able to reduce urban surface temperatures, the most effective measures are the ones that considered the application of cool roofs (green or white roofs). Although these two resilience strategies showed similar effectiveness in reducing urban temperatures under a future heat wave event, the scenarios than considered green roofing showed higher effectiveness in reducing the maximum temperature field. Oppositely, the resilience scenarios that considered the application of white roofs and the expansion of green urban areas showed higher ability to reduce nighttime urban temperatures, which can be very important for the buildings passive cooling and urban citizen's thermal comfort, allowing a relief from the daytime heat stress. All resilience scenarios produced a slight increase of the mean relative humidity fields, but given its small magnitude this fact is not expected to negatively impact the population thermal comfort. Considering the results showed by the white roofing approach, and that their application in urban buildings is a much cheaper and simpler process than the application of green roofs and/or the building of new urban parks, this resilience strategy can be seen as the most viable, cost-effective and economically attractive approach for mitigating urban extreme temperatures.

The addition of green urban areas produced very localized, but positive, effects. It should be borne in mind that although green/white roofs were applied in equivalent areas (approx. 75% of the urban area), the increase of urban parks was applied to a much smaller area (approx. 10% of the urban area) due to the unrealistic scenario that 75% of a given real urban location could be converted into green areas. Thus, it could be argued that if the application of all resilience scenarios would be assessed in terms of their effectiveness per area unit, urban green areas could show similar, or even higher, ability to reduce urban temperatures than the application of cool roofs. Moreover, and as highlighted by Li et al. (2014), in addition to the temperature reduction and consequent improvement of the urban population thermal comfort, measures that include the use of vegetated surfaces (green roofing and/or the increase of urban green areas) bring other advantages, not quantified in this study, such as improvements in air quality due to the conversion of CO_2 in O_2, reduction in photochemical activity (Li et al., 2010; Yang et al., 2008) and potential reduction in peak stormwater runoff (Berndtsson, 2010).

It is expected that the application effects of the tested resilience measures will vary with the synoptic/local scale weather conditions, geographical and topographical local characteristics, and also with other characteristics of the urban centre under study (materials used in the buildings and roads, characteristics of the urban areas, etc.). Although these effects can vary from city to city, the findings of this study can serve as a sound and grounded case study concerning the investigation of resilience strategies to mitigate extreme urban heat under climate change scenarios, which are expected to exacerbate the frequency and intensity of extreme meteorological phenomena. In addition to the urban population thermal stress mitigation, the adoption of this type of resilience measures brings other advantages such as substantial energy savings because less energy is spent in cooling interior buildings, since the adjacent outdoors are cooler. Moreover, the large-scale application of these types of resilience measures will significantly contribute for the mitigation of air pollution. On the one side, the lower energy demands for building cooling will mean lower emissions of CO_2, NOx and particulate matter (mainly PM10) produced by electrical power plants (Synnefa et al., 2008). On the other side, the increase of urban green areas and application of vegetated surfaces will mean conversion of CO_2 in O_2 due to photosynthesis. In addition, given that the production of hazardous urban ozone smog and its precursors is favoured by high temperatures, lowering urban heat will mitigate its formation. It was proven that, for the case of Los Angeles, an air temperature decrease of 1.5–2 °C using the resilience measures considered in the present study resulted in an ozone smog decrease of about 10–20% (Taha et al., 1997).

4. Conclusions

Due to anthropogenic climate changes, Porto is an urban area highly exposed to a future increase of the frequency, duration and magnitude of heat waves. Given the importance and impacts of such extreme meteorological events in the urban population health and life quality, it becomes vital to propose and assess the effectiveness of several resilience strategies in reducing urban heat under future heat waves episodes. For this purpose, several resilience scenarios were studied considering different resilience factors such as the

increase of urban green areas, the application of green and white roofs on Porto urban perimeter. The application of these resilience strategies and their effectiveness was estimated through numerical simulations with the WRF urban modelling system, using as case-study a future heat wave occurring in Porto urban area between 24 and 26 of July 2049. Meteorological initial and boundary conditions data were extracted from a climatic database built with the WRF model forced by the CMIP5 earth system model MPI-ESM considering RCP 8.5 future climate projections (Marta-Almeida et al., 2016), while high-resolution urban terrain and land use information was taken from the SRTM project (topography), the CORINE project and the European Environmental Agency Porto Urban Atlas (land use/land cover).

Results showed that the most effective resilience strategies are the ones that considered the application of cool roofs (green or white). These resilience strategies produced the highest reduction in the average and maximum surface temperature fields over Porto urban area under a future heat wave. The expansion of urban green areas also produced a reduction in the urban temperature fields, albeit very localized, but it should be borne in mind that this resilience scenario was applied to a much smaller area than the cool roofs scenarios. Given the fact that white roofs are typically easier and cheaper to apply in urban areas than green roofs, this resilience strategy can be seen as the most viable, cost-effective and economically attractive approach to mitigate extreme urban temperatures. Besides the temperature reduction and consequent improvement of the urban population thermal comfort, green roofing and/or the increase of urban green areas bring other advantages such has improved urban life quality, lower air pollution, energy savings and reduction in peak stormwater runoff.

Although the effects of the tested resilience strategies can be different for other locations, the present study was able to propose several different strategies to increase urban resilience to high temperature episodes such as heat waves, to prove their effectiveness in reducing urban heat and thus improve the thermal comfort of Porto urban population, to compare and quantify their ability to mitigate extreme temperatures in Porto urban environment. In addition, the application of such resilience measures will also positively influence urban air quality and favour air pollution mitigation in urban environments. Such findings can be of great importance for Porto urban planning stakeholders and decision-makers, given the expected increase in the heat waves frequency and intensity in future climate projections.

Acknowledgements

This work was supported by the project CLICURB - Urban atmospheric quality, climate change and resilience (EXCL/AAG-MAA/0383/2012-FCOMP-027379), funded by the European Regional Development Fund (ERDF) through the programme COMPETE and by the Portuguese Foundation for Science and Technology (FCT). The authors also wish to thank FCT for financing the post-doctoral grant of H. Martins (SFRH/BPD/66874/2009).

References

Basara, B.J., Basara, H.G., Illston, B.G., Crawford, K.C., 2010. The impact of the urban heat island during an intense heat wave in Oklahoma City. Adv. Meteorol. 10, 230365.

Berndtsson, J.C., 2010. Green roof performance towards management of runoff water quantity and quality: a review. Ecol. Eng. 36, 351–360.

Borrego, C., et al. (Eds.), 2015. CLICURB - Qualidade da Atmosfera Urbana, Alterações Climáticas e Resiliência. Departamento de Ambiente e Ordenamento, Centro de Estudos do Ambiente e Mar, Universidade de Aveiro 52 pp.

Brands, S., Herrera, S., San-Martin, D., Gutierrez, J.M., 2011. Validation of the ENSEMBLES global climate models over southwestern Europe using probability density functions, from a downscaling perspective. Clim. Res. 48 (2–3), 145–161.

Brands, S., Herrera, S., Fernández, J., Gutiérrez, J.M., 2013. How well do CMIP5 Earth System Models simulate present climate conditions in Europe and Africa? Clim. Dyn. 41 (3–4), 803–817.

Büttner, G., Feranec, G., Jaffrain, G., 2000. Corine Land Cover Update 2000, Technical Guidelines, EEA Technical Report No. 89.

Chen, F., Kusaka, H., Bornstein, R., Ching, J., Grimmond, C.S.B., Grossman-Clarke, S., Loridan, T., Manning, K.W., Martilli, A., Miao, S., Sailor, D., Salamanca, F.P., Taha, H., Tewari, M., Wang, X., Wyszogrodzki, A.A., Zhang, C., 2011. The integrated WRF/urban modelling system: development evaluation and applications to urban environmental problems. Int. J. Climatol. 31, 273–288.

Cheval, S., Dumitrescu, A., Bell, A., 2009. The urban heat island of Bucharest during the extreme high temperatures of July 2007. Theor. Appl. Climatol. 97 391-40.

EC, 2015. European Comission - Towards an EU Research and Innovation policy agenda for Nature-Based Solutions & Re-naturing Cities. Final Report of the Horizon 2020 Expert Group on 'Nature-Based Solutions and Re-Naturing Cities'. 2015. Publications Office of the European Union, Luxembourg ISBN 978-92-79-46051-7.

EEA, 2011. European Environment Agency - Green Infrastructure and Territorial Cohesion: The Concept of Green Infrastructure and its Integration into Policies Using Monitoring Systems. 2011. Publications Office of the European Union, Luxembourg ISBN 978-92-9213-242-2.
Farr, T.G., et al., 2007. The shuttle radar topography mission. Rev. Geophys. 45, RG2004 http://dx.doi.org/10.1029/2005RG000183.
Founda, D., Pierros, F., Petrakis, M., Zerefos, C., 2015. Inter-decadal variations and trends of the urban Heat Island in Athens (Greece) and its response to heat waves. Atmos. Res. 161-162, 1–13.
Giorgetta, M.A., Jungclaus, J., Reick, C.H., Legutke, S., Bader, J., Bottinger, M., Brovkin, V., Crueger, T., Esch, M., Fieg, K., 2013. Climate and carbon cycle changes from 1850 to 2100 in MPI-ESM simulations for the Coupled Model Intercomparison Project phase 5. J. Adv. Model. Earth Syst. 5 (3), 572–597.
IPCC AR5, 2013. In: Stocker, T.F., Qin, D., Plattner, G.-K., Tignor, M., Allen, S.K., Boschung, J., Nauels, A., Xia, Y., Bex, V., Midgley, P.M. (Eds.), Climate Change 2013: The Physical Science Basis. Contribution of Working Group I to the Fifth Assessment Report of the Intergovernmental Panel on Climate Change. Cambridge University Press, Cambridge, United Kingdom and New York, NY, USA 1535 pp.
Kharin, V., Zwiers, F.W., 2000. Changes in the extremes in an ensemble of transient climate simulations with a coupled atmosphere-ocean GCM. J. Clim. 13 (21), 3760–3788.
Kusaka, H., Kondo, H., Kikegawa, Y., Kimura, F., 2001. A simple single-layer urban canopy model for atmospheric models: comparison with multi-layer and slab models. Bound.-Layer Meteorol. 101, 329–358.
Kusaka, H., Kimura, F., 2004. Coupling a single-layer urban canopy model with a simple atmospheric model: Impact on urban heat island simulation for an idealized case. J. Meteorol. Soc. Jpn. 82, 67–80.
Lau, K.K., Lindberg, F., Rayner, D., Thorsson, S., 2015. The effect of urban geometry on mean radiant temperature under future climate change: a study of three European cities. Int. J. Biometeorol. 59 (7), 799–814.
Li, D., Bou-Zeid, E., 2013. Synergistic interactions between urban heat islands and heat waves: the impact in cities is larger than the sum of its parts. J. Appl. Meteorol. Climatol. 52, 2051–2064.
Li, J.F., Wai, O.W.H., Li, Y.S., Zhan, J.M., Ho, Y.A., Li, J., Lam, E., 2010. Effect of Green Roof on Ambient CO2 Concentration Building and Environment. 45 pp. 2644–2651.
Li, D., Bou-Zeid, E., Barlage, M., Chen, F., Smith, J.A., 2013. Development and evaluation of a mosaic approach in the WRF-Noah framework. J. Geophys. Res.-Atmos. 118, 1–18.
Li, D., Bou-Zeid, E., Oppenheimer, M., 2014. The effectiveness of cool and green roofs as urban heat island mitigation strategies. Environ. Res. Lett. 9, 055002.
Marta-Almeida, M., Teixeira, J., Carvalho, M., Melo-Gonçalves, P., Rocha, A., 2016. High resolution WRF climatic simulations for the Iberian Peninsula: Model validation. Phys. Chem. Earth, Parts A/B/C 94 (1474-7065):94–105. (August) http://dx.doi.org/10.1016/j.pce.2016.03.010.
Monteiro, A., Velho, S., 2014. Health heat stress in the Porto metropolitan area – a matter of temperature or inadequate adaptation? J. Geol. Soc. Berl. 145 (1–2).
Monteiro, A., Fonseca, L., Almeida, M., Sousa, M., Velho, S., Carvalho, V., 2012. Atlas da saúde e da doença. Vulnerabilidades climáticas e socioeconómicas. 1.
Monteiro, A., Carvalho, V., Oliveira, T., Sousa, C., 2013. Excess mortality and morbidity during the July 2006 heat wave in Porto, Portugal. Int. J. Biometeorol. 57 (1), 155–167.
Oke, T.R., Crowther, J.M., McNaughton, K.G., Monteith, J.L., Gardiner, B., 1989. The micrometeorology of the urban forest [and discussion]. Philos. Trans. R. Soc. Lond. Ser. B Biol. Sci. 324 (1223), 335–349.
Papangelis, G., Tombrou, M., Dandou, A., Kontos, T., 2012. An urban "green planning" approach utilizing the weather research and forecasting (WRF) modeling system. A case study of Athens, Greece. Landsc. Urban Plan. 105 (1–2), 174–183.
Persinger, M.A., 1980. The Weather Matrix and Human Behavior. Praeger, New York 327 pp.
Pineda, N., Jorba, O., Jorge, J., Baldasano, J.M., 2004. Using NOAA AVHRR and SPOT VGT data to estimate surface parameters: application to a mesoscale meteorological model. Int. J. Remote Sens. 25 (1), 129–143.
Russo, S., Dosio, A., Graversen, R.G., Sillmann, J., Carrao, H., Dunbar, M.B., Singleton, A., Montagna, P., Barbola, P., Vogt, J.V., 2014. Magnitude of extreme heat waves in present climate and their projection in a warming world. J. Geophys. Res. Atmos. 119 (12), 500–512.
Santos, J., Corte-Real, J., 2006. Temperature extremes in Europe and wintertime large-scale atmospheric circulation: HadCM3 future scenarios. Clim. Res. 3 (1), 3–18.
Shin, H.H., Dudhia, J., 2016. Evaluation of PBL parameterizations in WRF at subkilometer grid spacings: turbulence statistics in the dry convective boundary layer. Mon. Weather Rev. 144 (3), 1161–1177.
Skamarock, W.C., Klemp, J.B., Dudhia, J., Gill, D.O., Barker, D.M., Huang, X.Y., 2008. A Description of the Advanced Research WRF Version 3. NCAR Technical Note. Mesoscale and Microscale Meteorology Division of NCAR.
Spronken-Smith, R.A., Oke, T.R., 1998. The thermal regime of urban parks in two cities with different summer climates. Int. J. Remote Sens. 19 (11), 2085–2104.
Susca, T., 2012. Enhancement of life cycle assessment (LCA) methodology to include the effect of surface albedo on climate change: comparing black and white roofs. Environ. Pollut. 163, 48–54.
Synnefa, A., Dandou, A., Santamouris, M., Tombrou, M., Soulakellis, N., 2008. On the use of cool materials as a heat island mitigation strategy. J. Appl. Meteorol. Climatol. 47, 2846–2856.
Taha, H., Douglas, S., Haney, J., 1997. Mesoscale meteorological and air quality impacts of increased urban albedo and vegetation. Energy Build. 25 (2), 169–177.
Taylor, K.E., Stouffer, R.J., Meehl, G.A., 2012. An overview of CMIP5 and the experiment design. Bull. Am. Meteorol. Soc. 93 (4), 485–498.
Watkiss, P., Horrocks, L., Pye, S., Searl, A., Hunt, A., 2009. Impacts of Climate Change in Human Health in Europe. PESETA-human Health Study. Office for Official Publications of the European Communities, Luxembourg.
Wyngaard, J.C., 2004. Toward numerical modeling in the "terra incognita.". J. Atmos. Sci. 61, 1816–1826.
Yang, J., Yu, Q., Gong, P., 2008. Quantifying air pollution removal by green roofs in Chicago Atmos. Environment 42, 7266–7273.
Yang, J., Wang, Z.-H., Chen, F., Miao, S., Tewari, M., Voogt, J.A., Myint, S., 2015. Enhancing hydrologic modelling in the coupled weather research and forecasting - urban modelling system. Bound.-Layer Meteorol. 155, 87–109.
Zhou, B., Simon, J.S., Chow, F.K., 2014. The convective boundary layer in the terra incognita. J. Atmos. Sci. 71, 2545–2563.